# Surface State Magnetization and Chiral Edge States on Topological Insulators

Fan Zhang,* C. L. Kane, and E. J. Mele

*Department of Physics and Astronomy, University of Pennsylvania, Philadelphia, Pennsylvania 19104, USA*

(Received 14 August 2012; published 25 January 2013)

We study the interaction between a ferromagnetically ordered medium and the surface states of a topological insulator with a general surface termination that were identified recently [F. Zhang *et al.* Phys. Rev. B **86**, 081303(R) (2012)]. This interaction is strongly crystal face dependent and can generate chiral states along edges between crystal facets even for a *uniform* magnetization. While magnetization parallel to quintuple layers shifts the momentum of the Dirac point, perpendicular magnetization lifts the Kramers degeneracy at any Dirac points *except* on the side face, where the spectrum remains gapless and the Hall conductivity switches sign. Chiral states can be found at any edge that *reverses* the projection of the surface normal to the stacking direction of quintuple layers. Magnetization also weakly hybridizes noncleavage surfaces.

DOI: 10.1103/PhysRevLett.110.046404 PACS numbers: 71.70.Ej, 73.20.−r, 73.22.Gk, 73.43.−f

*Introduction.*—Since the discovery of topological insulators (TIs) [1–9], there has been tremendous interest in their topologically protected surface states. Previous work has focused mainly on the cleavage surfaces of $Bi_2Se_3$ or similar TIs with $R\bar{3}m$ symmetry that host spin-momentum locked helical metals. Interestingly, a quantum anomalous Hall (QAH) effect can be induced by exchange coupling the surface electrons to a magnetic insulator that lifts the Kramers degeneracy at the surface Dirac point (DP). When the magnetization is perpendicular to the quintuple layers (QLs), this introduces a mass term into the cleavage surface state Hamiltonian, and, if the Fermi energy is in this gap, there is a half-integer quantized Hall conductivity $\sigma_H = e^2/2h$ whose sign is determined by the direction of perpendicular magnetization. Theory predicts a 1D chiral edge state on the $Bi_2Se_3$ cleavage surface along a domain wall where the perpendicular magnetization reverses direction [1,4,10]. The fabrication of such an interface that displays the QAH effect poses a formidable experimental challenge.

In this Letter, we consider the effects of magnetic exchange coupling to topological surface states for a *general* crystal termination and discover new geometries that generically host 1D chiral edge channels. By breaking $\mathcal{T}$ symmetry, the surface magnetization (i) shifts the DP off $\mathcal{T}$-invariant momenta, (ii) couples noncleavage surfaces, and (iii) lifts the Kramers degeneracy at any DP *except* on the side face where the Hall conductivity switches sign. We find that all three effects are crystal face dependent. Surprisingly, 1D gapless chiral states can be induced at crystal edges *without* introducing a magnetic domain wall, accessing the QAH effect in a geometry that should be readily accessible to experiment. Interestingly, a recent experiment demonstrates bulk intergrowth of $Bi_2Se_3$ and the room temperature ferromagnet $Fe_7Se_8$ forms a "stack of cards" structure [11] that offers an opportunity for exploring the face-dependent interactions between TI surface states and ferromagnetic materials. Additionally, magnetically doped TIs show a ~40 meV gap [12,13] and a giant AH effect [14] on the cleavage surface, providing a large out-of-plane Zeeman field to engineer the QAH effect in our new geometries.

*Topological surface states.*—We start from a description of the low energy minimal model of $Bi_2Se_3$, followed by a derivation of the effective Hamiltonian of topological surface states near the DP of an arbitral face [15]. These apply generally to other TIs with $R\bar{3}m$ symmetry. Besides $\mathcal{T}$ and the parity inversion ($\mathcal{P}$) symmetries, $Bi_2Se_3$ crystal structure has a threefold rotational ($\mathcal{C}_3$) symmetry along $\hat{z}$ perpendicular to QLs and a twofold rotational ($\mathcal{C}_2$) symmetry along the $\bar{\Gamma}\bar{M}$ direction. We choose [16] the parity operator $\mathcal{P} = \tau_z$ and the time reversal operator $\mathcal{T} = iK\sigma_y$, where $K$ is the complex conjugate. To linear order in $k$, the $\boldsymbol{k}\cdot\boldsymbol{p}$ bulk Hamiltonian that preserves the above four symmetries has a unique form

$$\mathcal{H}_{\text{bulk}} = -m\tau_z + v_z k_z \tau_y + v_\parallel (k_y\sigma_x - k_x\sigma_y)\tau_x, \quad (1)$$

where we assume $v_z$, $v_\parallel > 0$. By matching the eigensystems of TI with $m > 0$ and vacuum with $m \to -\infty$, one can demonstrate the existence of topological surface states [15]. The DP solution is determined by the operators $\boldsymbol{S}_1$ and is free under any rotation of the operators $\boldsymbol{S}_2$. We first focus on the case with a crystal termination where the azimuthal angle is fixed ($\phi = 0$) and later generalize to situations where $\phi$ is allowed to vary between neighboring crystal facets. For an arbitrary face $\Sigma(\theta) \equiv \Sigma(\theta, \phi = 0)$ ($0 \le \theta \le \pi$) in Fig. 1, $\boldsymbol{S}_1$ and $\boldsymbol{S}_2$ pseudospins read

$$\begin{aligned} \boldsymbol{S}_1 &= \{\alpha\tau_x + \beta\sigma_y\tau_y, \alpha\tau_y - \beta\sigma_y\tau_x, \tau_z\}, \\ \boldsymbol{S}_2 &= \{\alpha\sigma_x - \beta\sigma_z\tau_z, \sigma_y, \alpha\sigma_z + \beta\sigma_x\tau_z\}, \end{aligned} \quad (2)$$

where $v_3 = \sqrt{(v_z\cos\theta)^2 + (v_\parallel\sin\theta)^2}$, $\alpha = v_z\cos\theta/v_3$, and $\beta = v_\parallel\sin\theta/v_3$. These pseudospins satisfy

 

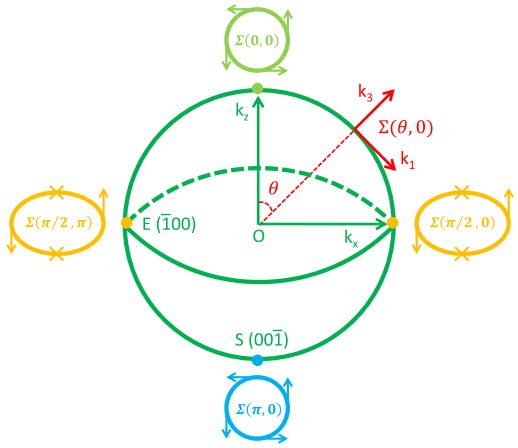


FIG. 1 (color online). The definition of crystal and local frames and the sketch of surface state conduction band *spin* textures. $\hat{k}_z$ is perpendicular to QLs. $\hat{k}_3$ is outwardly normal to the face $\Sigma(\theta, \phi)$, and $\hat{k}_1$ ($\hat{k}_2$) is in-plane tangent to the longitude (latitude) circle, with $\hat{k}_2 = \hat{k}_3 \times \hat{k}_1$. The spin textures described in the text are shown in local frames, with $\hat{k}_1$ toward the right and $\hat{k}_2$ toward the top.

$[S_a^i, S_b^j] = 2i\delta_{ab}\epsilon^{ijk}S_a^k$. We derive [15] the topological surface state Hamiltonian for face $\Sigma(\theta)$ to the linear order near DP,

$$\mathcal{H}(\theta) = v_1 k_1 S_2^y - v_\parallel k_y S_2^x, \tag{3}$$

where $v_1 = v_z v_\parallel / v_3$. The surface band is the negative eigenstate of $S_1^x$, and its chiral counterpart is localized on the opposite face. Thus, the surface state Hilbert space is reduced by half. The pseudospin ($\boldsymbol{S}_2$) texture of surface states on a general face is topologically equivalent to the helical metal found on the cleavage surface, although its energy dispersion is anisotropic in momentum. However, the *spin* texture is different for each face [15] and is determined by the bulk symmetries. As shown in Fig. 1, near the DP, the spin texture of a constant energy contour is helical only on the top ($\theta = 0$) and bottom ($\theta = \pi$) surfaces, is collapsed to one dimension on any side face ($\theta = \pi/2$), and is otherwise tilted out of plane. Interestingly, on a side face with normal $\hat{k}_x$, the spin texture is filtered into $\pm\hat{k}_y$ polarizations maximized at $k_y = 0$ and vanishing at $k_z = 0$. As a consequence, a Zeeman exchange field that couples to the physical spin $\sigma$ plays qualitatively different roles on different crystal faces.

Physically, a mass term $\Delta S_2^z$ or $\Delta S_2^z S_1^x$ in Eq. (3) is required to open an energy gap at the surface DP. This amounts to introducing either of the following external perturbations that break $\mathcal{T}$ symmetry:

$$\mathcal{H}_1^\Delta = \Delta_1(\alpha\sigma_z + \beta\sigma_x\tau_z), \qquad \mathcal{H}_2^\Delta = \Delta_2\sigma_z\tau_x. \tag{4}$$

The $\mathcal{H}_1^\Delta$ terms depend on the surface orientation through the $\theta$ dependence of $\alpha$ and $\beta$. On the cleavage surface ($\beta = 0$), this perturbation is a Zeeman term that can be induced by an exchange field, while on the side face ($\alpha = 0$) it becomes $\sigma_x\tau_z$, which is negligibly small [17] since it originates from the difference between the electron spin $g$ factors of Bi and Se [16]. In contrast, $\mathcal{H}_2^\Delta$ is independent of the crystal face angle but it requires a parity breaking interaction $\tau_x$ that seems to be infeasible.

*Surface magnetization effects.*—Now we consider a magnetic thin film with uniform magnetization that provides an exchange coupling $\boldsymbol{\Delta}\cdot\boldsymbol{\sigma}$ to the spin of TI surface states. Whether this breaking of the $\mathcal{T}$ symmetry opens a gap at the DP on face $\Sigma(\theta)$ is determined by whether it generates any of the perturbations listed in Eq. (4). Rewritten in the basis represented by $\boldsymbol{S}_1$ and $\boldsymbol{S}_2$, the exchange coupling can be decomposed as follows:

$$\Delta_x\sigma_x = \alpha\Delta_x S_2^x + \beta\Delta_x S_2^z S_1^z, \tag{5}$$

$$\Delta_y\sigma_y = \Delta_y S_2^y, \tag{6}$$

$$\Delta_z\sigma_z = \alpha\Delta_z S_2^z - \beta\Delta_z S_2^x S_1^z. \tag{7}$$

A topological surface state must be the negative eigenstate of $S_1^x$, and its positive counterpart is localized on the opposite face. Thus, the two fields proportional to $S_1^z$ couple the surface states on different noncleavage faces ($\beta \neq 0$). Although these two couplings play negligible roles as the TI dimension becomes larger than the surface state penetration length, they can be important for a sufficiently thin TI. As illustrated in Fig. 2, these two couplings hybridize the opposite surface states without opening any energy gap. The $S_2^x S_1^z$ term breaks up the two DPs that repel each other in the $\hat{k}_1$ direction, leading to two zero energy nodes at $v_z k_z = \pm\Delta_z$ and $k_y = 0$ [18]. The $S_2^z S_1^z$ field splits the two DPs in energy, resulting in a zero energy ellipse at $v_\parallel^2 k_y^2 + v_z^2 k_z^2 = \Delta_x^2$ [18].

For magnetization parallel to QLs, the induced exchange terms $\Delta_x S_2^x$ and $\Delta_y S_2^y$ do not contain any mass terms listed in Eq. (4) and thus do not open gaps at any surface DPs. Instead, they break $\mathcal{T}$ symmetry by shifting the DP from $\bar{\Gamma}$ to a non-$\mathcal{T}$-invariant momentum

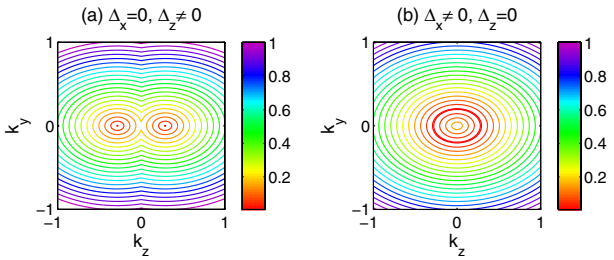


FIG. 2 (color online). Constant energy contour plot of the lowest conduction band of the hybridized surface states on two opposite side faces. (a) $\Delta_x = 0$, $\Delta_z = 0.2$; (b) $\Delta_x = 0.2$, $\Delta_z = 0$. We use arbitrary units, with $v_\parallel = 1$ and $v_z = 0.7$.

$$k_1 = -\frac{\Delta_y}{v_1}, \qquad k_y = \frac{\alpha\Delta_x}{v_\parallel}. \tag{8}$$

Equation (8) implies that magnetization only moves the DP on the side face in the $\pm\hat{k}_z$ direction. More generally, as the surface state helicities are opposite for opposite faces, the same magnetization moves their DPs in opposite directions in the crystal frame. Since a pair of opposite side faces is also connected by the rotational symmetry along $\hat{k}_z$, shifting the side face DPs is allowed along $\hat{k}_z$ and forbidden along $\hat{k}_y$.

As shown in Eq. (7), the magnetization perpendicular to QLs introduces a field $\alpha\Delta_z S_2^z$ that behaves as $\mathcal{H}_1^\Delta$. This mass breaks $\mathcal{T}$ symmetry by lifting the Kramers degeneracy, leading to a surface state gap $\sim 2\alpha\Delta_z$. Importantly, on the closed surface of a compact TI, this gap is face dependent: It is largest on the cleavage surface ($\alpha = \pm 1$) and it *vanishes* on the side face ($\alpha = 0$) where the mass switches sign.

*1D chiral edge states.*—We find that the momentum-space Berry curvature becomes nontrivial when $\mathcal{T}$ symmetry is broken by the mass term $\alpha\Delta_z S_2^z$. For an arbitrary face, the Berry curvature reads

$$\Omega_{\hat{k}_3}^{(s)}(\theta, k_1, k_y) = -\frac{s\alpha\Delta_z v_1 v_\parallel}{2\varepsilon^3}, \tag{9}$$

where $\varepsilon = \sqrt{v_1^2 k_1^2 + v_\parallel^2 k_y^2 + \alpha^2\Delta_z^2}$ and $s = +(-)$ denotes the surface conduction (valence) band. The momenta are measured from the shifted DP in Eq. (8) in the presence of parallel magnetization. The *orbital* magnetic moment [19,20] carried by a surface state Bloch electron is

$$m_{\hat{k}_3}^{(s)}(\theta, k_1, k_y) = -\frac{\alpha\Delta_z m_e v_1 v_\parallel}{\varepsilon^2}\mu_B, \tag{10}$$

where $m_e$ is the electron mass and $\mu_B$ is the Bohr magneton. Unlike the Berry curvature, the orbital magnetization is independent of the band index $s$. In the presence of an electric field in the surface plane, a surface state electron acquires an anomalous transverse velocity proportional to the Berry curvature [19,20], giving rise to an intrinsic Hall conductivity

$$\sigma_H = \frac{e^2}{2h}\left[\frac{\alpha\Delta_z}{\varepsilon(E_F)} - \mathrm{sgn}(\alpha\Delta_z)\delta_{s,+}\right], \tag{11}$$

where $E_F$ is the Fermi energy. Provided that $E_F$ lies in the surface gap, the surface band contributes $e^2/2h$ to the Hall conductivity, with the sign given by $\mathrm{sgn}(\alpha\Delta_z)$.

This Hall conductivity is half-integer quantized but with opposite signs for crystal faces with surface normals that have opposite $z$ projections (i.e., perpendicular to QLs), even though the surface magnetization is uniform. Since $\Delta\sigma_H = e^2/h$ across the interface, there must be a chiral edge state channel whenever there is an edge or a narrow side face that connects two faces whose surface normals have opposite $z$ projections. This is the *criterion* for the existence of chiral edge states in the presence of uniform $\Delta_z\sigma_z$ magnetization on the TI surface. Uniform magnetization may not be easy to realize, as the surface tends to produce easy axis anisotropy for the magnetic order. However, our proposal will be realized if the two easy axes have $z$ projections with the same sign.

We now propose three TI shapes that support chiral edge states in the presence of surface magnetization perpendicular to QLs and uniform on all relevant faces. For a spherical TI, shown in Fig. 3(a), the mass term and the Hall conductivity switch sign across the equator ($\alpha = 0$). Therefore, there is a chiral channel along the equator for gapless edge states. A TI slab depicted in Fig. 3(b) is topologically equivalent in shape to a spherical TI, with the upper (lower) hemisphere becoming the top (bottom) cleavage surface. Similarly, there is a gapless chiral state along the side faces when the exchange field effect dominates over the finite size effect. The QAH effect in this bilayer (BL) system, which has been studied before [10,21,22] and is a special case where our criterion applies, can be alternatively described in the crystal frame as follows:

$$\mathcal{H}_{BL} = v_\parallel(k_y\sigma_x - k_x\sigma_y)\tau_x - m_t\tau_z + \Delta_z\sigma_z, \tag{12}$$

where $\tau_x = \pm$ respectively represent the bottom and top surfaces and $m_t$ is a trivial mass due to finite size tunneling between the surfaces. We further obtain the four-band energy dispersions

$$\varepsilon_{BL} = \pm\sqrt{v_\parallel^2 k_\parallel^2 + (m_t \pm \Delta_z)^2}. \tag{13}$$

As the exchange field strength $\Delta_z$ is turned up from zero, the energy gap closes at $\Delta_z = \pm m_t$ and reopens, indicating the topological distinction between the magnetization-induced gap with respect to the tunneling-induced gap.

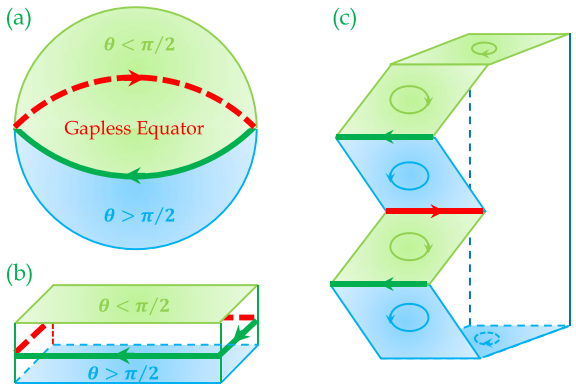


FIG. 3 (color online). Three TI shapes that support chiral edge states in the presence of a uniform exchange field $\Delta_z\sigma_z$ on the surface. (a) A spherical TI, (b) a TI slab, and (c) a TI with zigzag side faces. In all panels, the faces with $\theta < \pi/2$ ($\theta > \pi/2$) are colored in light green (cyan), and the chiral edge states are denoted by bold lines with arrows.

Further analysis using Eq. (11) shows that the two valence bands have a total $e^2/h$ contribution to $\sigma_{\mathrm{H}}$ when $|\Delta_z| > |m_t|$, leading to a QAH effect. This analysis applies generally to any other slab with $\theta \neq \pi/2$.

Our criterion also predicts chiral edge states on a TI with a more remarkable shape, as depicted in Fig. 3(c). In the intergrowth with a ferromagnet [11], a TI often has zigzag side faces. Each convex corner of the zigzag side connects an upper face with $\theta_N < \pi/2$ and a lower face with $\theta_S > \pi/2$, while a concave corner connects the two faces upside down. As a consequence, the zigzag side exhibits staggered edge states with opposite chiralities along the convex and concave corners. In the presence of an electric field perpendicular to the average zigzag side face, there will be a net chiral current carried by edge states at the convex or concave corners depending on the electric polarity, while, for an electric field perpendicular to QLs, edge states with opposite chiralities are both populated and the Hall currents become counterpropagating, canceling each other out, on average.

In the limit of $\theta_{N,S} \simeq \pi/2$, the surface state Hilbert spaces for the upper and lower faces are both the negative eigenstate of $S_1^x(\pi/2) = \sigma_y\tau_y$. The chiral corner states are also pseudospin filtered, since they satisfy $S_2^x(\pi/2) = \sigma_z\tau_z = \pm 1$, where the sign depends on the polarity of the $\Delta_z\sigma_z$ magnetization. These two features are analogous to the case of a magnetic domain wall deposited on the cleavage surface, where the chiral edge state is not only orbital chiral but also spin filtered.

In the opposite limit in which $\theta_N \simeq 0$ and $\theta_S \simeq \pi$, these zigzag side faces become a chain of staggered top and bottom cleavage surfaces, in which the two opposite edges of each face are joined respectively to the opposite edges of the neighboring upper and lower faces. Our proposed criterion can be applied to each pair of neighboring faces. The origin of their chiral corner states can also be intuitively understood by our previous analysis [Eq. (12)] designed for parallel surfaces. In such a limit, the top and bottom surface states have zero orbital overlap in the sense that they are negative and positive eigenstates of $\tau_x$, respectively. The chiral edge state is not spin filtered either because of the opposite helicities of the two surface states. These features are quite different from the situation for two joined side faces or with a magnetic domain wall on the cleavage plane.

We now turn on the azimuthal angle. Since the bulk crystal has $\mathcal{C}_3$ symmetry along $\hat{k}_z$ that upgrades to continuous rotational symmetry in linear order, we can set $\phi = 0$ along an arbitrary axis perpendicular to $\hat{z}$. But, more generally, for two crystal faces joined at an edge with normals along *different* azimuthal angles, we need to specify their difference $\Delta\phi$ to determine the chirality of their edge state. In fact, the criterion for the existence of a chiral edge state at a TI corner can be relaxed to $\theta(\Sigma_\sigma) < \pi/2$ and $\theta(\Sigma_{\bar{\sigma}}) > \pi/2$, with $\sigma = S$ or $N$, where $\Sigma_{S,N}(\theta, \phi)$ could even be curved faces or have different azimuthal angles. Figure 4 sketches a chiral state

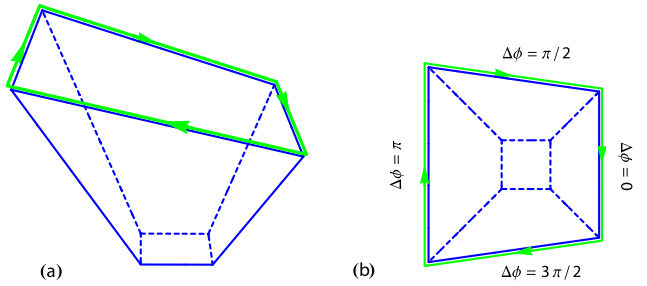


FIG. 4 (color online). (a) A schematic TI crystal that has a top face with $0 < \theta_t < \pi/2$, a bottom face with $\theta_b = \pi$, and four surrounding faces with the same $\theta_s$ and $\pi/2 < \theta_s < \pi$. (b) The top view of (a). When perpendicular magnetization is present, there is a chiral state along the edges of the top face but none on the bottom edges. The four surrounding faces have $\Delta\phi = \phi_s - \phi_t = 0$, $\pi/2$, $\pi$, and $3\pi/2$, respectively [47].

along the edges that connect a top face with four surrounding faces that have the same $\theta_s$ but different $\phi_s$.

*Discussions.*—In conclusion, we provide a general theory that allows a thorough understanding of the interaction of TI surface states with a ferromagnetically ordered medium, with a surprising criterion for the presence of a chiral edge state (QAH effect) with no need of magnetic anisotropy. This approach may also simplify the interferometry of Majorana fermions [23,24] that requires one to generate chiral edge states on the TI surface. Our proposed chiral edge states may be accessible by STM or in multiterminal transport at the corners of a TI zigzag side that form [11] in the intergrowth with a ferromagnet. Our work may shed light on cleavage surface transport experiments where it is crucial to minimize the influence from the side face, i.e., making samples in the square shape. On the other hand, this work also provides a new strategy for the fabrication of electronic devices that exploit the crystal face dependence of TI surface state phenomena. We thus suggest reexamining anomalies in existing data by taking into account the dependence of surface states on the surface orientation and look forward to more explorations on the noncleavage surfaces.

A Zeeman field that couples to spin could also be introduced by doping TIs with magnetic impurities [12–14,21,25–41] or partially by applying a parallel magnetic field [42,43] instead of depositing a ferromagnetic film [11,22,44–46] on the surface. With these experimental progresses, QAH effects are likely to occur when their TI samples are fabricated in geometries similar to Fig. 3 or Fig. 4. We have noticed that a very special case of our proposed physics, i.e., a QAH effect in a magnetic doped $Bi_2Se_3$ slab with only two cleavage surfaces [10,21,22] and thickness less than six QLs, has been demonstrated by the first-principles calculations [21]. While observing QAH effects in thin films is still experimentally challenging, our newly discovered criterion does not necessarily require such a limited geometry and constitutes a significant advance. Finally, we point out that the surface magnetization

can be built into the topological boundary condition of TIs as a family of surface potentials [15] that break $\mathcal{T}$ symmetry but preserve $\mathcal{P}$ symmetry.

This work has been supported by DARPA under Grant No. SPAWAR N66001-11-1-4110.

*zhf@sas.upenn.edu


[1] L. Fu, C. L. Kane, and E. J. Mele, Phys. Rev. Lett. **98**, 106803 (2007); L. Fu and C. L. Kane, Phys. Rev. B **76**, 045302 (2007).

[2] J. E. Moore and L. Balents, Phys. Rev. B **75**, 121306 (2007).

[3] R. Roy, Phys. Rev. B **79**, 195322 (2009).

[4] M. Z. Hasan and C. L. Kane, Rev. Mod. Phys. **82**, 3045 (2010).

[5] X. Qi and S. Zhang, Rev. Mod. Phys. **83**, 1057 (2011).

[6] D. Hsieh, D. Qian, L. Wray, Y. Xia, Y. Hor, R. Cava, and M. Hasan, Nature (London) **452**, 970 (2008).

[7] H. Zhang, C. Liu, X. Qi, X. Dai, Z. Fang, and S. Zhang, Nat. Phys. **5**, 438 (2009).

[8] Y. Xia, D. Qian, D. Hsieh, L. Wray, A. Pal, H. Lin, A. Bansil, D. Grauer, Y. S. Hor, R. J. Cava, and M. Z. Hasan, Nat. Phys. **5**, 398 (2009).

[9] Y. Chen, J. G. Analytis, J. Chu, Z. Liu, S. Mo, X. Qi, H. Zhang, D. Lu, X. Dai, Z. Fang, S. Zhang, I. R. Fisher, Z. Hussain, and Z. Shen, Science **325**, 178 (2009).

[10] X. L. Qi, T. L. Hughes, and S. C. Zhang, Phys. Rev. B **78**, 195424 (2008).

[11] H. Ji, J. M. Allred, N. Ni, J. Tao, M. Neupane, A. Wary, S. Xu, M. Z. Hasan, and R. J. Cava, Phys. Rev. B **85**, 165313 (2012).

[12] Y. Chen, J. Chu, J. Analytis, Z. Liu, K. Igarashi, H. Kuo, X. Qi, S. Mo, R. Moore, D. Lu, M. Hashimoto, T. Sasagawa, S. Zhang, I. Fisher, Z. Hussain, and Z. Shen, Science **329**, 659 (2010).

[13] S. Xu *et al.*, Nat. Phys. **8**, 616 (2012).

[14] C. Chang, J. Zhang, M. Liu, Z. Zhang, X. Feng, K. Li, L. Wang, X. Chen, X. Dai, Z. Fang, X. Qi, S. Zhang, Y. Wang, K. He, X. Ma, and Q. Xue, arXiv:1108.4754.

[15] F. Zhang, C. L. Kane, and E. J. Mele, Phys. Rev. B **86**, 081303(R) (2012).

[16] The effective Hilbert space near the bulk gap is spanned by states with angular momentum (proportional to the electron spin) $\sigma = \pm 1/2$ and $p_z$ orbitals $\tau_z = \pm 1$. The $\tau_z = 1$ $(-1)$ orbital is dominated by states from Bi (Se) atoms, due to the large energy difference between $4p$ (Se) and $6p$ (Bi) principal quantum levels. These two states are inverted at the $\Gamma$ point due to spin-orbital couplings.

[17] This has to be determined by experiments. Our edge state criterion still holds by turning off $\Delta_x$, even though the $\sigma_x\tau_z$ field turns out to be comparable to the $\sigma_x$ field.

[18] Here $\Delta_{x,z}$ are reduced due to the small overlap of surface states on opposite faces in the surface normal direction.

[19] D. Xiao, M. Chang, and Q. Niu, Rev. Mod. Phys. **82**, 1959 (2010).

[20] F. Zhang, J. Jung, G. A. Fiete, Q. Niu, and A. H. MacDonald, Phys. Rev. Lett. **106**, 156801 (2011).

[21] R. Yu, W. Zhang, H. Zhang, S. Zhang, X. Dai, and Z. Fang, Science **329**, 61 (2010).

[22] Q. Meng, S. Vishveshwara, and T. L. Hughes, Phys. Rev. Lett. **109**, 176803 (2012).

[23] L. Fu and C. L. Kane, Phys. Rev. Lett. **102**, 216403 (2009).

[24] A. R. Akhmerov, J. Nilsson, and C. W. J. Beenakker, Phys. Rev. Lett. **102**, 216404 (2009).

[25] Y. S. Hor, P. Roushan, H. Beidenkopf, J. Seo, D. Qu, J. G. Checkelsky, L. A. Wray, D. Hsieh, Y. Xia, S. Y. Xu, D. Qian, M. Z. Hasan, N. P. Ong, A. Yazdani, and R. J. Cava, Phys. Rev. B **81**, 195203 (2010).

[26] J. Cha, J. Williams, D. Kong, S. Meister, H. Peng, A. Bestwick, P. Gallagher, D. Goldhaber-Gordon, and Y. Cui, Nano Lett. **10**, 1076 (2010).

[27] L. Wray, S. Xu, Y. Xia, D. Hsieh, A. Fedorov, Y. Hor, R. Cava, A. Bansil, H. Lin, and M. Hasan, Nat. Phys. **7**, 32 (2011).

[28] Y. Okada, C. Dhital, W. Zhou, E. D. Huemiller, H. Lin, S. Basak, A. Bansil, Y. B. Huang, H. Ding, Z. Wang, S. D. Wilson, and V. Madhavan, Phys. Rev. Lett. **106**, 206805 (2011).

[29] K. Nomura and N. Nagaosa, Phys. Rev. Lett. **106**, 166802 (2011).

[30] H. Jin, J. Im, and A. J. Freeman, Phys. Rev. B **84**, 134408 (2011).

[31] C. Niu, Y. Dai, M. Guo, W. Wei, Y. Ma, and B. Huang, Appl. Phys. Lett. **98**, 252502 (2011).

[32] Y. H. Choi, N. H. Jo, K. J. Lee, J. B. Yoon, C. Y. You, and M. H. Jung, J. Appl. Phys. **109**, 07E312 (2011).

[33] P. Haazen, J. Laloë, T. Nummy, H. Swagten, P. Jarillo-Herrero, D. Heiman, and J. Moodera, Appl. Phys. Lett. **100**, 082404 (2012).

[34] G. Rosenberg and M. Franz, Phys. Rev. B **85**, 195119 (2012).

[35] T. M. Schmidt, R. H. Miwa, and A. Fazzio, Phys. Rev. B **84**, 245418 (2011).

[36] J. Honolka, A. Khajetoorians, V. Sessi, T. Wehling, S. Stepanow, J. Mi, B. Iversen, T. Schlenk, J. Wiebe, N. Brookes, A. Lichtenstein, Ph. Hofmann, K. Kern, and R. Wiesendanger, Phys. Rev. Lett. **108**, 256811 (2012).

[37] Z. Salman, E. Pomjakushina, V. Pomjakushin, A. Kanigel, K. Chashka, K. Conder, E. Morenzoni, T. Prokscha, K. Sedlak, and A. Suter, arXiv:1203.4850.

[38] Jian-Min Zhang, Wenguang Zhu, Ying Zhang, Di Xiao, and Yugui Yao, Phys. Rev. Lett. **109**, 266405 (2012).

[39] D. Zhang, A. Richardella, S. Xu, D. Rench, A. Kandala, T. Flanagan, H. Beidenkopf, A. Yeats, B. Buckley, P. Klimov, D. Awschalom, A. Yazdani, P. Schiffer, M. Hasan, and N. Samarth, Phys. Rev. B **86**, 205127 (2012).

[40] S. Qiao, Z. Liu, F. Ji, Bin Li, F. Xi, K. Kuroda, M. Ye, K. Miyamoto, and A. Kimura (unpublished).

[41] L. Zhao, Z. Chen, and L. Krusin-Elbaum (unpublished).

[42] S. Pershoguba and V. Yakovenko (unpublished).

[43] F. Zhang and A. H. MacDonald, Phys. Rev. Lett. **108**, 186804 (2012).

[44] I. Garate and M. Franz, Phys. Rev. Lett. **104**, 146802 (2010).

[45] T. Yokoyama, Y. Tanaka, and N. Nagaosa, Phys. Rev. B **81**, 121401(R) (2010).

[46] P. Wei, F. Katmis, B. Assaf, D. Heiman, P. Jarillo-Herrero, and J. Moodera (unpublished).

[47] We illustrate the case $\theta_t + \theta_s < \pi$ in this figure. The case of $\theta_t + \theta_s > \pi$ or a concave side corner can be considered similarly. For the special case of $\theta_t + \theta_s = \pi$ and $\Delta\phi = \pi$, Eq. (12) applies here.